



HAL
open science

An urban thermal tool chain to simulate summer thermal comfort in passive urban buildings

Adrien Toesca, Damien David, André Kuster, Michel Lussault, Kevyn Johannes

► To cite this version:

Adrien Toesca, Damien David, André Kuster, Michel Lussault, Kevyn Johannes. An urban thermal tool chain to simulate summer thermal comfort in passive urban buildings. *Building and Environment*, 2022, 215, pp.108987. 10.1016/j.buildenv.2022.108987 . hal-03633803

HAL Id: hal-03633803

<https://hal.science/hal-03633803v1>

Submitted on 7 Apr 2022

HAL is a multi-disciplinary open access archive for the deposit and dissemination of scientific research documents, whether they are published or not. The documents may come from teaching and research institutions in France or abroad, or from public or private research centers.

L'archive ouverte pluridisciplinaire **HAL**, est destinée au dépôt et à la diffusion de documents scientifiques de niveau recherche, publiés ou non, émanant des établissements d'enseignement et de recherche français ou étrangers, des laboratoires publics ou privés.

An urban thermal tool chain to simulate summer thermal comfort in passive urban buildings

Adrien Toesca^a, Damien David^{a,1}, André Kuster^a, Michel Lussault^b, Kévyen Johannes^a*

5 ^a *University of Lyon, INSA Lyon, CNRS, CETHIL, UMR5008, 69621 Villeurbanne, France*

^b *University of Lyon, UMR 5600 EVS, Lyon, France*

Abstract

10 This paper presents a simulation tool chain for the prediction of thermal comfort in passive urban buildings during summer and under heat wave conditions. The tool chain encompasses EnergyPlus building energy model and the Urban Weather Generator and UrbaWind tools to consider the impacts of the urban environment on building loads. This chain of tools is computationally efficient and does not require notable expertise for the simulations. To assess its accuracy, this simulation results are compared to in situ measurements. This paper describes the measurement setup, analyzes the measurement results and reveals a satisfactory model accuracy through a comparison

* This is to indicate the corresponding author.

Email address: damien.david@insa-lyon.fr

Address: Bâtiment Sadi-Carnot, 9, Rue de la Physique, Campus LyonTech La Doua, 69621-Villeurbanne cedex, France

Abbreviations

UTTC	Urban Thermal Tool Chain
UHI	Urban Heat Island
AFN	Airflow Network
UCM	Urban Canopy Model
UWG	Urban Weather Generator
DSM	District-Scale Model
MMM	Micrometeorological Model
CFD	Computational Fluid Dynamics
UBEM	Urban Building Energy Model
RMSE	Root Mean Square Error

to the measurement data. The average nighttime urban heat island between July and September 2020 reached 2.31 °C in the city of Lyon. Not considering the urban heat island effect (employing rural weather files) in urban thermal simulations could induce a 1 °C bias in indoor air temperature predictions. This could also result in overpredicting the cooling potential of natural ventilation during summer. Key parameters of the simulation accuracy are identified. These are the action schedule of occupants in regard to opening devices (shutters, windows and doors) and the urban boundary layer height at night.

25 *Keywords:* Building thermal simulation, in situ measurements, heatwave, urban environment, simulation tool chain, urban heat island, occupant behavior

1. Introduction

Under global warming, climatic events such as heatwaves will be longer, more frequent and more intense. This issue will become increasingly critical in cities since heat waves are amplified by the urban heat island (UHI) phenomenon. Air temperatures in cities are likely to become increasingly unbearable. Extreme urban temperatures could impact a fair majority of the worldwide population since, according to the World Bank (2018) [1], nearly 56% of the worldwide population lives in urban areas, with a net increasing trend over the past decades. Extreme temperatures could cause discomfort and health issues in urban outdoor environments and within urban buildings.

This is especially true in passive urban buildings. A building is passive when no active cooling system ensures acceptable indoor comfort levels during summer periods. According to Santamouris (2018) [2], the penetration of active cooling systems in the residential sector approached 8% across Europe in 2006. Consequently 92% of the total residential buildings were passive buildings when exposed to summer climate conditions. The social benefits of increasing the penetration rate of active cooling systems are questionable because cooling systems consume energy and discharge hot air into building surroundings. In passive buildings, occupants only rely on passive cooling strategies to reach acceptable indoor comfort levels. These strategies are

obviously much less robust than are active cooling systems, which makes passive buildings more vulnerable to excessively hot outdoor conditions.

Thermal comfort in passive urban buildings during heat wave events or more generally under hot summer conditions must be addressed. Appropriate building simulation tools are needed to accurately predict indoor thermal comfort in passive urban buildings. The purpose of this paper is to propose an appropriate simulation tool.

This paper is organized as follows: the second section develops the model requirements and reviews similar existing tools. The proposed simulation tool is described in the third section of this paper. A measurement campaign was conducted in four apartments located in the city of Lyon (France) during the summer of 2020. The measurements produced reference data employed to assess the accuracy of the proposed model. Details on the measurement campaign are provided in the fourth section of this paper. Measurement results are described in the fifth section. Simulation outputs are compared to the measurement data in the sixth section of this paper. The final section examines specific aspects of the model accuracy and relevance.

2. Model Requirements and Existing Tools

The developed building thermal model must fulfill two requirements: the algorithm must accurately model all the predominant heat transfer rates occurring in a given passive building under summer conditions, and the model must consider the effect of the surrounding urban environment.

2.1 Passive Building Thermal Behavior Under Summer Conditions

Thermal regulation of a passive building is entirely ensured by the actions of the occupants ([3] Fabi et al., 2012). Certain actions directly affect the building thermal characteristics. These actions correspond to the opening of windows for natural ventilation and the activation of solar shading systems [4, 5, 6, 7]. Other actions modify the distribution and amplitude of the internal gains within buildings. Under hot

conditions, an occupant might prefer to remain in cooler rooms, or they may avoid the utilization of gas cookers [4, 5, 6, 7].

75 Under summer conditions, solar radiation constitutes one of the major thermal stresses on buildings ([8] Levermore et al., 2000). The manner in which solar radiation heats buildings greatly depends on the shading effects of surrounding solar masks (topography, surrounding buildings, trees, balconies, etc.) and on window characteristics (optical properties, dimensions, nature and use of the employed shading devices).

80 Under summer conditions, the air temperature difference between the indoor and outdoor environments is smaller than that under winter conditions, but heat exchange between indoor and outdoor air is intensified when windows are opened to enable natural ventilation. The cooling rate resulting from natural ventilation is highly sensitive to the outdoor air temperature and the wind pressure loads on the facade.

85 The building thermal models implemented in popular simulation software packages, such as TrnSys ([9] Solar Energy Laboratory, 2007) or EnergyPlus ([10] U.S. Department of energy, 2014), already contain submodels to simulate specific aspects of the summer thermal behavior of a given building. These models contain advanced windows and shading models, with the possibility of providing schedules to control the opening rate. These software packages offer full control of the related internal heat production of occupants. They contain, or they propose in the form of an additional module, an airflow network (AFN) model to predict natural ventilation flow rates and
90 corresponding thermal effects.

2.2 Effect of the Urban Fabric on the Outdoor Thermal Conditions

95 Building thermal loads are computed based on outdoor meteorological quantities: the temperature, humidity and velocity of the outdoor air, incoming diffuse and beam solar radiation, and incoming thermal radiation. All these parameters are available in weather data files. However, the weather data contained in weather data files are representative of the outdoor thermal conditions in rural areas.

100 Initially, building thermal models compute building thermal loads directly based on
rural weather data. These models employ air temperature and velocity values to
compute external convection on the building facade, and solar and thermal radiation are
projected onto the building facade. Progressively, building thermal models have
incorporated new features to simulate the effects of building surroundings. Currently,
105 EnergyPlus and TrnSys can adjust the outdoor velocity with a configurable velocity
profile. These models contain specific options to simulate the effects of outdoor solar
masks.

These features remain insufficient to simulate all the urban effects on building
thermal loads, especially the effects impacting the outdoor temperature and wind loads,
110 which play a predominant role in passive building thermal behavior under summer
conditions ([8] Levermore et al., 2000). Thus, dedicated models must be applied in
conjunction with a building thermal model to accurately simulate the thermal behavior
of urban buildings.

In the following two sections, the effects of the urban environment on the outdoor
115 thermal conditions are detailed, and the models dedicated to the simulation of these
effects are listed. These two sections provide the required background to justify the
architecture of the proposed tool chain. Two length scales of the urban thermal effects
are distinguished: city-scale effects and district-scale effects.

2.3 City-scale Effects

120 City-scale effects include wind profile adjustment, urban heat island (UHI)
phenomenon, and reduction in incoming solar radiation due to urban pollution.

Wind profile adjustment entails vertical wind profile adaptation to variations in the
surface roughness between rural and urban areas. EnergyPlus proposes a simple
analytical model based on power wind profiles to simulate wind profile adjustment. The
125 Urban Weather Generator ([11] Bueno et al. 2013) contains a more detailed model,
which can simulate urban breeze-induced wind flows.

The urban heat island effect influences the bulk air temperature and bulk air
humidity. The bulk air temperature is the average air temperature within the urban

canopy and within a perimeter of a few hundreds of meters. The evolution of the bulk
130 air temperature and humidity between rural and urban areas is determined by variations
in the land surface energy budget, which is attributable to variations in land surface
materials, building densities, and building shapes.

UHI effects are simulated with specific models, namely, urban canopy models
(UCMs). A survey of the existing UCMs was reported by Grimmond (2010) [12].
135 UCMs can be applied online (coupled with a full mesoscale atmospheric model) or
offline (thermal solicitations on the city are directly extracted from weather data files).
The latter option is more computationally efficient, but this approach is less accurate
because the evolution of the air temperature in the urban boundary layer is not modeled.
A compromise was developed by Bueno et al. (2013) [11], who combined a UCM and
140 a simplified thermal model to capture the urban boundary layer. Their model was
implemented in a simulation tool denoted as the Urban Weather Generator (UWG).

Pollution accumulation attenuates solar radiation. Ferreira et al. (2012) [13] studied
the variation in the incoming shortwave radiation at the surface in urban areas and
reported a reduction varying between 1% (per year) and 22% (during the wet season)
145 in different urban areas worldwide. Solar radiation attenuation provides favorable
conditions for a passive building to maintain acceptable indoor conditions because there
is less heat to evacuate. A clean sky represents the worst-case scenario in regard to the
thermal behavior of a passive building. Moreover, no specific tool has been developed
to consider the pollution effect on solar loads for building simulation purposes.

150 *2.4 District-scale Effects*

District-scale effects correspond to shorter gradients within a perimeter of a few
building blocks. At this scale, we consider the explicit effect of each urban feature
(building, road, tree, or furniture) on the outdoor thermal environment. The wind flow
is adjusted around urban buildings and furniture, forming complex three-dimensional
155 flow conditions. The air temperature and humidity distributions are influenced by local
phenomena, such as air stagnation in shaded areas or hot air discharge from air
conditioning systems. Solar radiation loads on buildings depend on interbuilding

shading and reflection effects. Thermal radiation loads on buildings also depend on interbuilding radiation heat exchange because the visibility of the sky vault is severely
160 reduced by the presence of surrounding buildings.

In the present paper, all the models employed to simulate district-scale thermal effects are referred to as district-scale models (DSMs). DSMs simulate the various heat transfer processes between and within buildings. The literature provides a great diversity of DSMs, with varying precision levels.

165 DSMs with the highest precision level are often referred to as micrometeorological models (MMMs). Examples of MMMs include SOLENE-Microclimate ([14] Musy et al., 2015), EnviBatE ([15] Gros et al., 2016), and ENVI-Met ([16] Bruse et al., 1998). These models primarily aim to predict the outdoor comfort level. As such, these models must estimate values of all the outdoor thermal parameters at any point in the outdoor
170 volume. These estimations require at least a 3D computational fluid dynamics (CFD) model and an accurate radiation heat exchange model.

DSMs with an intermediate precision level are referred to as urban building energy models (UBEMs). An example UBEM is City-SIM ([17] Robinson et al., 2009) and ([18] Frayssinet, 2018). UBEMs primarily strive to predict aggregated or statistical
175 quantities representing the thermal behavior of the entire building stock. The most common output parameter is the aggregated power consumption. Compared to MMMs, UBEMs do not rely on CFD models to predict outdoor air flows. UBEMs simulate interbuilding radiation heat exchange with a coarser mesh size across urban surfaces.

DSMs with a low precision level include nodal models of single urban patterns in
180 UCMs, such as an idealized urban canyon. In this model category, groups of individual buildings are clustered in representative equivalent buildings. The urban canyon model of the town energy balance model ([19] Masson, 2000) was applied as a DSM, coupled with a building energy model by ([20] Bueno et al. 2012) and ([21] Ali-Toudert et Böttcher, 2018).

185 Finally, CFD models may be adopted in the preprocessing simulation step to evaluate pressure and convection heat transfer coefficients along building facades. Due to the Reynolds invariance phenomenon ([22] Van Hooff, 2010), only a limited number of simulations is needed to cover all possible incoming wind speed and direction values. When applied for this purpose, CFD models can be considered DSMs because they

190 simulate building interactions at the district scale. General-purpose CFD models might
be employed as DSMs, but dedicated tools such as UrbaWind ([23] Fahssis et al., 2010)
have also been developed to simplify model parametrization.

It should be mentioned that all DSMs contain building thermal models. However,
none of these building thermal models are as detailed as EnergyPlus or TrnSys, and
195 none can accurately predict the indoor comfort conditions within passive buildings.
Thus, for the purpose of the present paper, DSMs are applied to refine the thermal loads
on a single building of interest ([24] Lauzet et al., 2019).

It should also be mentioned that MMMs require high computer resources. The
possibility of performing long-term simulations with MMMs is rather limited.
200 Moreover, all DSMs except EnviBatE remain under development within the research
community. Managing these models requires notable expertise.

2.5 Limits of the Existing Urban Thermal Simulation Tool Chains

Lauzet et al. (2019) [24] provided a broad overview of existing tool chains for the
simulation of the thermal behavior of urban buildings. The inventoried tool chains could
205 be classified into two categories: tool chains involving an MMM for the simulation of
district-scale effects and tool chains without an MMM.

Tool chains involving an MMM provide accurate and exhaustive representations of
the district thermal state. However, since these tool chains require high computational
resources, only short simulation periods are conceivable. Merlier et al. (2017) [25] only
210 performed 2-day simulations with a tool chain comprising SOLENE-Microclimate
(DSM) and BuildSysPro (BEM). Yang et al. (2012) [26] only performed 3-day
simulations in ENVI-Met (DSM + BEM).

The other tool chains can perform one-year simulations on a personal computer.
However, none of these tool chains are explicitly dedicated to the prediction of thermal
215 comfort in buildings. They are designed to predict heating and cooling power demands,
either given a single urban building or a group of buildings. Salvati et al. (2015) [27]
applied a tool chain including UWG and EnergyPlus to predict the energy demand of
buildings located in Rome and Barcelona. Palme et al. (2017) [28] employed a tool

chain including UWG and TrnSys to estimate the cooling demand of different types of
220 residential buildings during a summer period of 3 months. Bueno et al. (2011) [29]
implemented a full coupling scheme between TEB and EnergyPlus, but their intention
was to refine the representative building model within TEB. They did not strive to
obtain an accurate representation of the thermal behavior of a specific building. Indoor
comfort predictions require a much more accurate representation of heat exchange
225 across the envelope of the building of interest.

3. Description of the Proposed Simulation Tool

As mentioned in the introduction of the previous section, the developed simulation
tool must accurately simulate all the predominant heat transfer rates occurring in a
passive building under summer conditions, and it must consider the effect of the
230 surrounding urban environment. One additional restriction was added in the
development of this simulation tool: the tool must be user-friendly to promote adoption
by a majority of actors in the building energy simulation community. Thus, the tool
must not require advanced programming skills to be implemented. The tool should be
based on robust existing software, for which full documentations, and eventually a user-
235 friendly interface, are available.

The simulation tool proposed in this paper encompasses a chain of three simulation
tools: Urban Weather Generator ([11] Bueno et al. 2013), UrbaWind ([24] Fahsis et
al., 2010), and EnergyPlus ([9] U.S. Department of energy, 2014). The Urban Weather
Generator is available as a Python library in a dedicated GitHub repository. UrbaWind
240 is a commercial software package with a user-friendly interface. EnergyPlus is a free
program for which several user-friendly interfaces are available. These three tools are
robust, and their validation has been the subject of several publications.

The phenomena considered by the chain of tools at the different urban scales are
graphically shown in Figure 1. At the building scale, the thermal behavior of the
245 building of interest is simulated with EnergyPlus, which contains an AFN for the
simulation of natural ventilation airflow.

At the district scale, pressure coefficients are provided by UrbaWind. EnergyPlus simulates the solar shading attributed to surrounding buildings. District-scale effects on the other outdoor thermal quantities, such as the air temperature and humidity and thermal radiation, are not modeled. This limitation is mainly attributed to the way
250 EnergyPlus considers the outdoor environment. EnergyPlus accepts only one outdoor air temperature value and one humidity value, given by the input weather file. EnergyPlus cannot take advantage of refined representations of the surrounding air temperature and humidity distributions.

255 For the model of the outdoor thermal radiation distribution at the district scale, a compromise was made between user friendliness and accuracy. Since version 8.8, EnergyPlus allows to enter manually the temperature schedules and the view factors associated to the building surrounding surfaces. To obtain surface temperature schedules, a dedicated DSM is needed. To obtain view factors, a dedicated routine must
260 be implemented. These additional features could drastically increase the level of complexity of the simulation tool. Since outdoor thermal radiation heat exchange was not identified as a key heat transfer rate of the passive building thermal behavior under summer conditions [8], it was decided to retain the default algorithm of EnergyPlus to compute the outdoor thermal radiation heat exchange process.

265 At the city scale, the analytical model of EnergyPlus was adopted to predict wind profile adjustment values between the rural area and urban environment. The Urban Weather Generator simulates the dynamic urban heat island effect. To perform simulations under the worst-case scenario, solar radiation attenuation due to atmospheric particles is neglected.

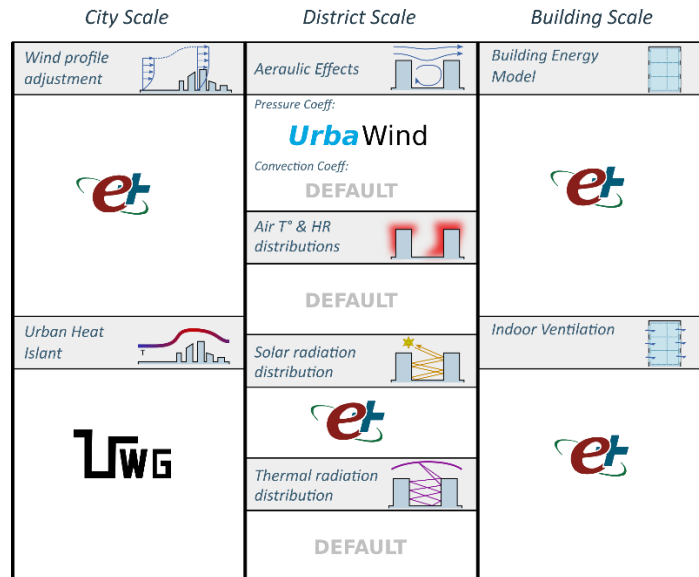


Figure 1: Urban effects modeled by the urban thermal tool chain

The pressure coefficients provided by UrbaWind are computed with a wind velocity value obtained at a fixed height (usually, the building height is chosen) along the urban air velocity profile ([24] Fahssis et al., 2010). However, the EnergyPlus AFN model
 275 considers the velocity value at the local opening height to compute pressure loads based on the above pressure coefficients. To overcome this discrepancy, a homogeneous vertical velocity profile was implemented in EnergyPlus, with a velocity value corresponding to the velocity at the building height.

The developed simulation tool was denoted as an Urban Thermal Tool Chain
 280 (UTTC). This new designation clarifies the distinction that must be made between UBEMs and the present tool. The target outputs of UBEMs are statistical or aggregated quantities pertaining to a whole building stock. The target outputs of the UTTC include detailed indoor comfort parameters of a single building. UBEMs do not require detailed building thermal models because of the bulk effect: when aggregating building-related
 285 quantities, the errors made in regard to each building are compensated. Obviously, the building model of the UTTC must be very detailed to obtain detailed indoor comfort quantities.

The term tool chain refers to the coupling strategy between the abovementioned three simulation tools. Two coupling strategies are available: two-way (or strong) coupling

290 and one-way coupling (or chaining). The first strategy entails orchestrating information exchange between the simulation tools at every time step. In this manner, heat transfer rates at the building surface, which are finely estimated with the building simulation model, can be communicated to a given DSM or UCM to refine the outdoor thermal environment prediction process. The implementation of this coupling strategy requires advanced programming skills. Its advantages are rather limited when the target quantities are building indoor thermal parameters. Thus, we adopted a one-way coupling strategy: information is transferred from larger scales to smaller scales, as shown in Figure 2. UrbaWind provides pressure coefficient tables which are then implemented in EnergyPlus, either manually through a dedicated user interface, or through the EnergyPlus Python library (eppy). UWG transforms the rural weather data contained in input weather files (EPW format) according to a parametric description of a given town. It produces urban weather files (EPW format), which can be read directly by EnergyPlus. By that way, the transfer of information between UWG and EnergyPlus can be ensured manually, and no auxiliary program is needed. UWG only modifies the outdoor dry temperature, dewpoint temperature, and relative humidity. Section 6.1 describes how the UWG input parameters were determined for the present study.

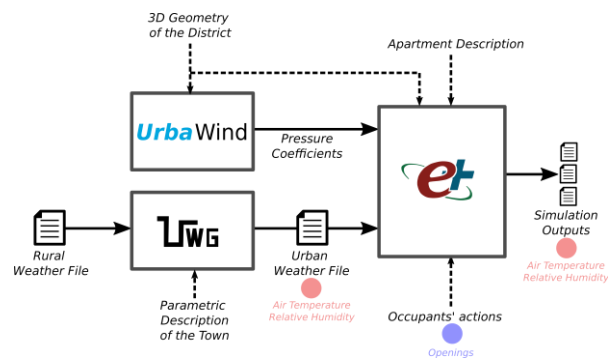


Figure 2: Transfer of information within the urban thermal tool chain, including categories of measurements (the blue dots indicate the measured simulation input data; the red dots indicate the measurements employed to assess the accuracy of the simulation tool chain)

4. Measurement Campaign

The Urban Thermal Tool Chain (UTTC) must be confronted to measurement data to assess the accuracy of indoor thermal ambiance predictions in passive urban buildings under hot summer meteorological conditions. An in situ measurement campaign was conducted in Lyon during the summer of 2020 from July to September to collect measurement data. The measurement campaign is detailed in this section.

4.1 Case Studies

To cover the diversity of urban fabrics and building designs encountered in typical French cities, four apartments stemming from different construction periods were selected as case studies. The four construction periods are:

- Canut period: early 19th century.
- Industrial period: between the late 19th century and the early 20th century.
- Reconstruction period: the period right after the Second World War.
- Contemporary period: the period when the characteristics of new buildings adhered to the requirements of French thermal regulation RT2012.

Figure 3 shows, for each study case apartment, an aerial photograph of the surrounding district in which the blue rectangle identifies the location of the apartment, and a floor plan of the apartment.

The Canut-period building is located in the 4th arrondissement of Lyon. In this district, the urban morphology is dense. The building is located on a hill, and nothing blocks the solar radiation and wind originating from the south direction. The Canut apartment is located on the 4th floor out of 6. Its outdoor wall is thick (approximately 0.5 m). The building is made of stone, with a thin layer of thermal insulation on the inside face added during renovation. The apartment is a mono-oriented structure. Its unique façade faces the south direction.

The Industrial-period building is located in the 3rd arrondissement of Lyon. In this district, the urban morphology includes closed blocks. The Industrial-period apartment is located on the 6th floor out of 7. Its outdoor walls are made of concrete, with a thermal

340 insulation layer on the inside face. The apartment is a west-facing mono-oriented
 apartment. The apartment faces the core volume of the block.

345

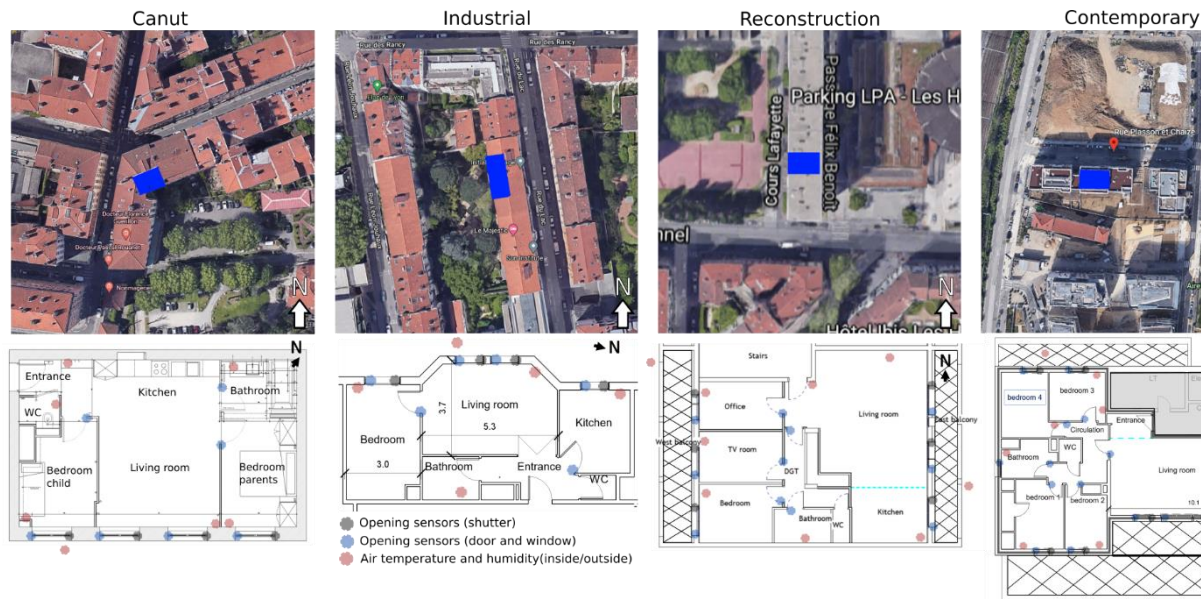


Figure 3: Urban environment around the case study buildings (the blue rectangle corresponds to the studied apartment), apartment floor plans and sensor locations ([30] Google maps, 2021)

The Reconstruction-period building is located in the 3rd arrondissement of Lyon.
 350 Here, the urban morphology consists of large ensembles. This building is less dense
 than the previous case study buildings, which could result in higher exposure of the
 building to solar radiation and wind loads. The Reconstruction-period apartment is
 located on the 7th floor out of 16. The apartment is an east/west-oriented apartment.

The Contemporary-period building is located in the 9th arrondissement of Lyon,
 355 where the urban morphology encompasses detached collective buildings. The urban
 morphology around the Contemporary-period building is less dense than the urban
 morphology around the other test case buildings, which could result in higher exposure
 of the building to solar radiation and wind loads. This building is also located more

toward the outskirts of the city and not at the city center as are the other buildings. The
360 Contemporary-period apartment is located on the top floor of the building. The walls
are made of concrete with a thermal insulation layer thicker than that in the previous
test cases. The apartment is a north/south-oriented apartment.

4.2 *Sensors and Sensor Locations*

The sensor distributions within the four apartments are shown in the floor plans
365 depicted in Figure 3.

The opening actions of the occupants (blinds, doors and windows) were measured
with binary contact sensors. Each window was equipped with two contact sensors: one
sensor to detect window opening actions and one sensor for the blinds. Each door was
equipped with one contact sensor. Additionally, the occupants of each apartment were
370 required to periodically answer a survey regarding their habits and were interviewed at
the end of the measurement campaign. These surveys and interviews were intended to
reconstitute the schedule of the occupants' behavior in case of measurement failures.

To help interpret the behavior of the occupants in regard to external windows,
continuous recording of the outdoor sound level was performed along the façades of
375 the Canut-, Reconstruction-, and Contemporary-period apartments. No acoustic
measurement was performed along the façade of the Industrial-period apartment
because it faced the core volume of a closed building block, where the noise pollution
level was low.

The outdoor air temperature was monitored to determine the relevance of urban heat
380 island (UHI) predictions. Each apartment was equipped with one or two shaded outdoor
air temperature and humidity sensors (1 sensor for the Industrial- and Canut-period
apartments and 1 sensor on each side of the Reconstruction- and Contemporary-period
apartments). The air temperature and humidity were measured in all the rooms of the
apartments (the red dots in Figure 3). The indoor temperature and humidity sensors
385 were vertically fixed at the center of the room to compensate for vertical stratification
on shaded walls or furniture surfaces to avoid direct sun exposure.

Brand, model and accuracy information of the sensors is listed in Table 1. All sensors, except acoustic sensors, communicated data through a gateway under the ENOCEAN protocol. The gateway transferred these data to an online server via a 4G key. The sensors transmitted data to the gateway each time the recorded variation in the measured quantities exceeded the trigger resolution indicated in the last column of the table.

Table 1: Sensor specifications

Measured quantity	Sensor model/brand	Accuracy	Trigger resolution
Internal temperature and humidity	-/Nodon	$\pm 0.16\text{ }^{\circ}\text{C} \pm 2\%$	$\pm 0.1\text{ }^{\circ}\text{C}$
External temperature and humidity	FAFT60/Eltako electronics	$\pm 0.3\text{ }^{\circ}\text{C} \pm 5\%$	$\pm 0.1\text{ }^{\circ}\text{C}$
Manipulation of doors and windows	-/Nodon	-	State change
Manipulation of shutters	TRIO2SYS/O2LINE	-	State change
Sound level	GREENBEE/azimuth-monitoring	$\pm 0.1\text{ dB}$	
Sound level	SV 258 Pro/SVANTEK	$\pm 0.1\text{ dB}$	

4.3 Dates of the Simulation Campaign

The measurements were performed during the summer of 2020. The campaign began on the 3rd of July and ended near mid-October.

5. Measurement Results

During the measurement campaign, the wind speed at the rural weather station remained above 2 m/s during 60% of the time. The wind direction mainly included the north and south directions.

5.1 Outdoor Temperatures

Figure 4 shows 2 graphs for each case study apartment. The upper graph shows measured outdoor air temperature values measured by the urban in situ outdoor sensors (blue line) and by the rural weather station (green line). The bottom graph shows the

UHI amplitude δ_{UHI} computed based on the measured outdoor temperatures (blue line). The UHI amplitude δ_{UHI} is the difference between the urban and rural temperatures:

$$\delta_{UHI} = T_{o,urb} - T_{o,rur}$$

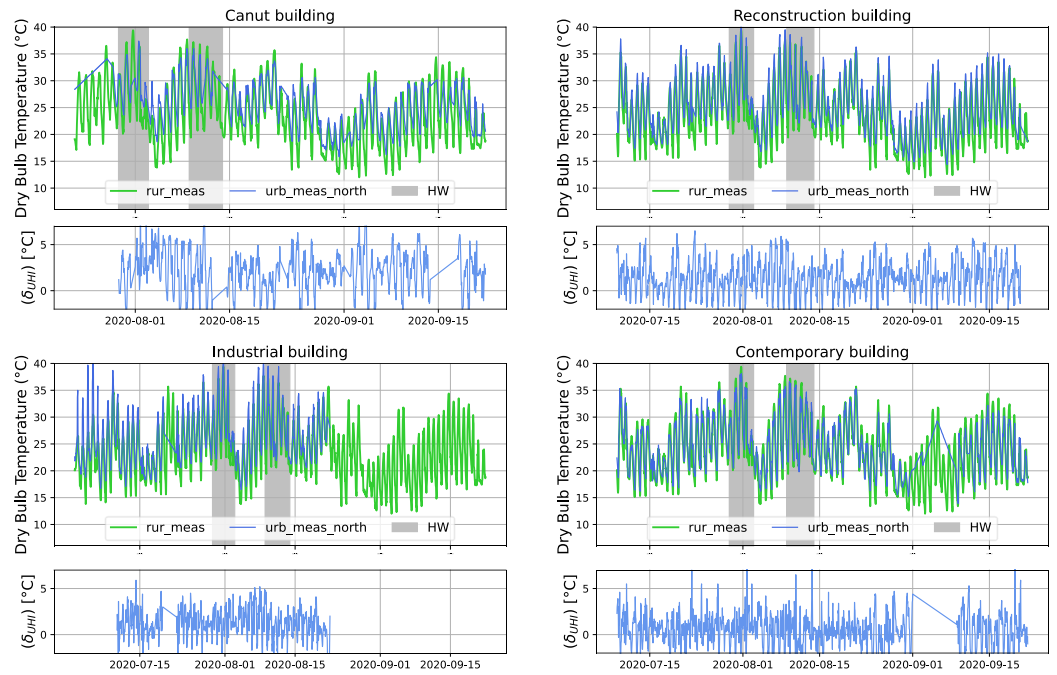
Measurement failures occurred during the measurement campaign. Certain sensors
410 experienced battery depletion during long periods. These periods are identifiable on the graphs through long-term linear evolutions. The outdoor sensor of the Industrial-period building experienced battery depletion from the 21st of August until the end of the measurement campaign. Almost no measurement data were collected by the sensors located on the east side of the Reconstruction-period apartment and on the south side
415 of the Contemporary-period building. Additionally, certain sensors measured abnormal temperature peaks during the day. These peaks were attributed to direct sunlight, which heated the sensor thermal shield. The temperature sensor near the Industrial-period building was particularly affected by direct sunlight. The other sensors were located in more shaded areas. These abnormal temperature peaks and missing values were not
420 considered in the subsequent analysis.

Two heat wave events were detected on the rural temperature profiles: between the 29th of July and the 2nd of August, and between the 8th and the 13th of August. These heat wave events are marked with gray rectangles in Figure 4. They were detected using the method from Pascal et al. (2006) [31]. During these heat wave events, the air
425 temperature increased above 34 °C and did not decrease below 20 °C over 3 consecutive days.

A comparison of the measured outdoor air temperatures between the rural area (green) and urban area (blue) reveals the evolution of the UHI effect. The UHI amplitude δ_{UHI} was close to 0 °C during the daytime. UHI effects mostly occurred
430 during the nighttime, when δ_{UHI} could vary between 0 °C (near the 20th of August) and 5 °C. The UHI amplitude was slightly larger near the Canut-period building (top left curves), which is located in the densest district among the test cases. The UHI amplitude was slightly smaller near the Contemporary-period building (bottom right curves), which is located in the least dense district among the various test cases, close to the
435 Saone River, which is only 200 m from the building. The average nighttime values of the UHI amplitude $\overline{(\delta_{UHI})}_{night}$ were computed considering nighttime periods between

22:00 and 7:00. The values ranged from 1.12 °C (Contemporary-period building) to 3.34 °C (Canut-period building). The UHI effects were more intense during the night.

The average amplitudes of the daily temperature fluctuations $\overline{\Delta T_{o,meas}}$ are provided in Table 3. The average amplitude reached 12 °C in the rural area. The urban heat island effect reduced the temperature fluctuations near the Canut-, Reconstruction- and Contemporary-period buildings, with $\overline{\Delta T_{o,meas}}$ reaching 7 °C, 10.5 °C and 10.2 °C, respectively. Higher fluctuations near the Industrial-period building could be attributable to direct sunlight heat reaching the sensor during the day.



445

Figure 4: Outdoor air temperature measurement results are shown in the top graphs (urban measurements are indicated in blue lines and rural measurements obtained from Météo-France are indicated in green, and heat wave days are identified by gray rectangles), and the urban heat island amplitude δ_{UH1} is shown in the bottom graph (blue lines)

450 *5.2 Indoor Temperatures and Opening Schedules*

Figure 5 shows 2 graphs for each case study apartment. The upper graph shows the indoor temperatures within each room of the apartments. In each apartment, the temperature in the living room is indicated with a red line. The gray rectangles indicate the holiday periods during which the apartments remained unoccupied. A temperature
455 threshold of 28 °C is highlighted as an arbitrary comfort temperature threshold. The bottom graph shows the percentage of windows opened among the apartments and the outdoor sound levels. None of the shutter opening sensors functioned properly, which is why shutter opening percentages are not displayed.

Within each apartment, the room air temperatures exhibited similar trends. The daily
460 average values evolved simultaneously along the same direction. High or low fluctuations simultaneously affected all rooms. Two rooms exhibited particular air temperature evolution processes. The WC of the Canut-period apartment included a washing machine that periodically raised the room air temperature (blue line, top left curve). The living room of the Contemporary-period apartment was isolated from the
465 rest of the apartment, and its temperature evolution differed significantly (red line, bottom right curve).

The room air temperature evolution greatly depended on the window opening schedules. During the holiday periods (gray areas), all the windows and shutters remained closed. The apartments occurred in a configuration that minimized thermal
470 interactions with the outdoor environment. The daily temperature fluctuations were low, but the average daily temperatures were high because natural ventilation did not mitigate heat accumulation in the rooms.

Between the 16th and 28th of August, the windows of the Canut-period apartment remained open all the time. This continuous opening state resulted in the maximum
475 daily temperature fluctuations observed throughout the entire measurement campaign.

Daily window opening schemes were recorded during significant periods in the Industrial- and Contemporary-period buildings. The occupants closed windows and shutters during the day, progressively opened windows and doors during the evening and left the windows in a few rooms open to ensure natural ventilation at night. The

480 associated temperature regimes included temperature stabilization during the daytime
 and temperature decline during the nighttime.

The average amplitudes of the daily air temperature fluctuations in the living rooms
 reached 2.5 °C, 2 °C, 1,6 °C and 1.6 °C for the Canut-, Industrial-, Reconstruction- and
 Contemporary-period apartments, respectively. The indoor fluctuations were 5.5 times

485 lower than the outdoor fluctuations on average.

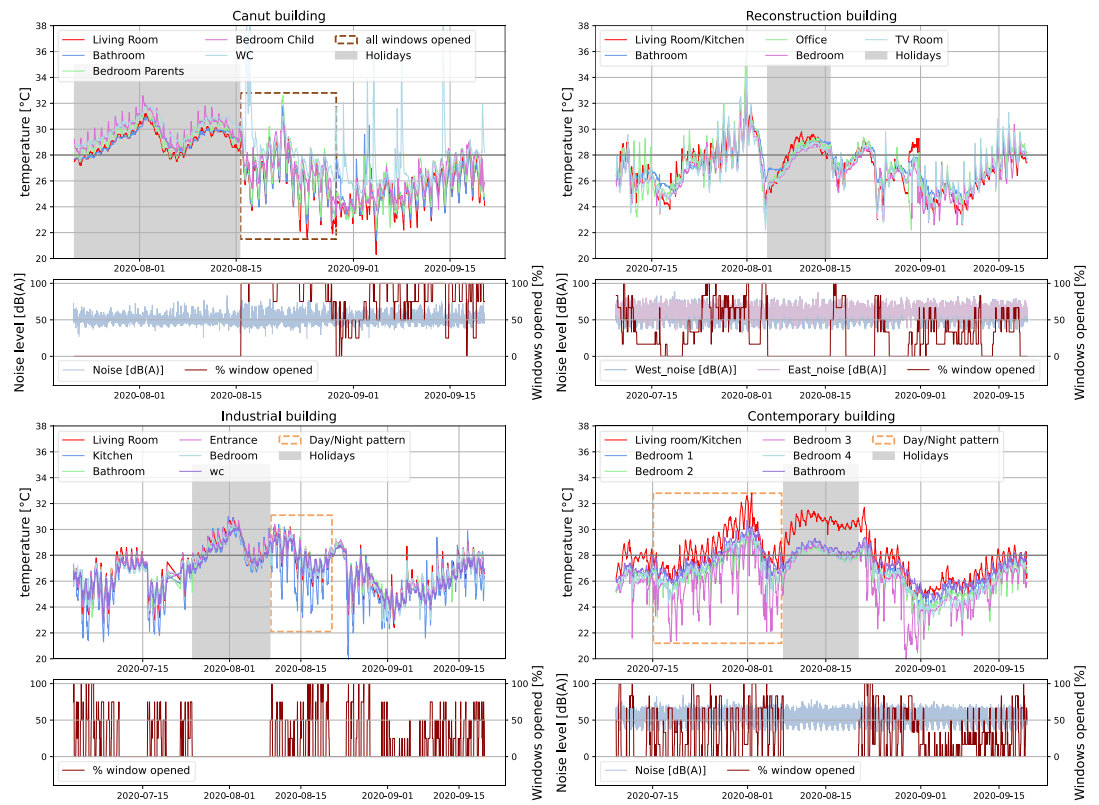


Figure 5: Measured indoor air temperature, holiday periods (gray rectangles), continuous window opening state (brown dashed-line rectangles) and daily window opening schemes (orange dotted-line rectangles) (top curves), noise levels and percentage of windows opened (bottom curves) for each case study apartment

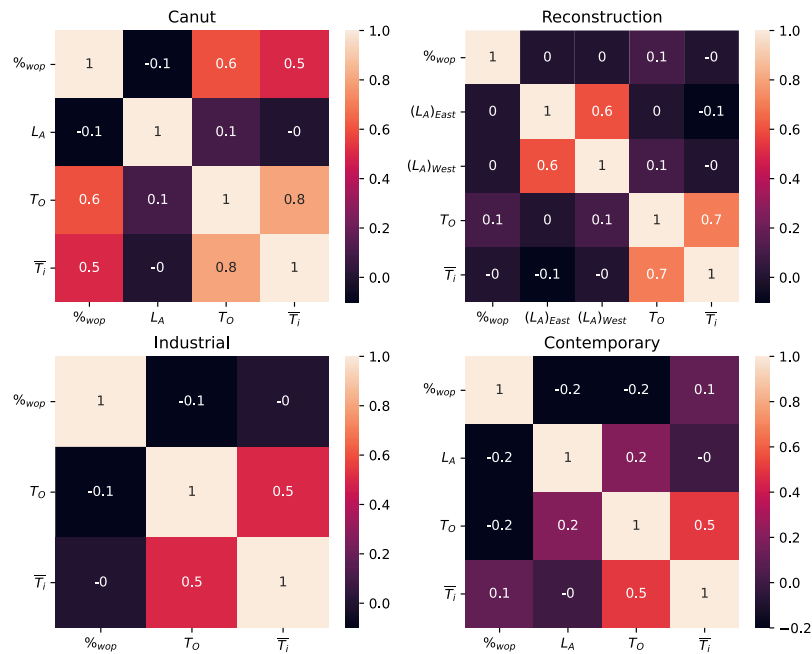
490 *5.3 Interpretation of the Window-opening Behavior*

From a purely thermal perspective, the ideal window opening behavior would consist of opening windows whenever the outdoor temperature is lower than the indoor temperature to ensure that natural ventilation is always employed for cooling purposes. However, this ideal behavior was rarely observed for several reasons. The occupants
495 were not always available to open windows, either because they were sleeping or because they were absent from the apartment. Opening windows could also expose the indoor environment to external pollution, especially noise.

As a first attempt to interpret the window opening schedules, a correlation matrix between the percentage of the opening schedule $\%_{wop}$, noise level L_A , outdoor
500 temperature T_o and average indoor temperature among the various apartment rooms \overline{T}_i was computed from the measurement data obtained in the four apartments. The holiday periods were removed from this analysis. The resulting correlation matrix is shown in Figure 6.

The correlation values between $\%_{wop}$ and L_A were very low. It might be expected
505 that windows would be closed more often under a high outdoor noise level. This behavior was not observed during the measurement campaign. This does not suggest that the occupants did not consider noise pollution. This indicates that their decision to open or close windows was not triggered by variations in the outdoor noise level but by variations in their degree of noise acceptance, which depended on the nature of their
510 activities (cooking, sleeping, watching TV, etc.).

The correlation values between $\%_{wop}$ and T_o or \overline{T}_i were very low, except for the Canut-period apartment. These correlation values reflect the relationship between the window opening state and both the daily and day-to-day variations in the temperature. Temperature variations did not seem to trigger window opening decisions. The higher
515 correlation values for the Canut-period apartment are attributed to a nearly constant opening state in July and August, when the outdoor air temperature was high, and a nearly constant closing state after mid-September, when the outdoor air temperature dropped. The opening state was thus correlated with day-to-day temperature variations.



520 *Figure 6: Correlation matrix (Pearson standard correlation coefficient) for the interpretation of the window opening schedules. $\%wop$: window opening schedules; L_A : outdoor noise level; T_O : outdoor air temperature; \bar{T}_i : average indoor air temperature (plotted with the `seaborn.heatmap()` function in the `seaborn` library in Python)*

6. Simulation Results

525 6.1 Model Settings and Simulation Inputs

Rural weather data were provided by Météo-France. All the data needed to compile an EPW weather file were collected at a weather station located near the Lyon-Bron

airport. The methodology of Taesler and Andersson (1984) [32] was applied to decompose the measured global solar radiation into diffuse and beam components.

530 Four different UWG input parameters files were produced for the four test cases. The list of UWG input parameters contains statistical parameters which describe the district within which the building is located. To determine the value of those parameters, data was collected over a 400m squared area around the building of interest. Information about the urban layout (building height, building density, vegetation and
535 tree density, etc.) was deduced from Google Maps data ([30] Google maps, 2021). The resulting input parameters are given in Table 2. Information about the building usage was extracted from metropolitan maps ([34] Open Data of the Métropole of Lyon). No guidelines were found for the appropriate settings of certain urban climate parameters, especially the urban boundary layer height during the daytime and nighttime, the
540 inversion height, the circulation and exchange coefficients. These parameters were adjusted to improve the agreement with outdoor temperature measurements.

In regard to UrbaWind, the urban geometry was directly extracted from Google Maps based on a 400-m square area near the apartments of interest.

Regarding EnergyPlus, the apartment shapes and dimensions were measured in situ,
545 modeled in 3 dimensions in Revit software and exported to DesignBuilder to establish corresponding EnergyPlus models. EnergyPlus was applied with its AFN and the Full Exterior Solar option. Pressure coefficients obtained from UrbaWind were manually entered in the DesignBuilder interface. Default DesignBuilder parameters for the residential buildings were applied to determine the internal load in each room. The wall
550 compositions of the Contemporary-period apartment were fully described in architect-provided floor plans. The wall compositions of the other apartments were deduced from the building wall composition database Tabula ([34] Rochard, 2015) and in situ observations. Window and door opening schedules were directly determined from the measured data and implemented in EnergyPlus. As mentioned earlier, almost all the
555 contact sensors targeting the blinds failed. Blind opening schedules were produced based on the results of occupants' interviews. These schedules were adjusted to improve the agreement between the simulation results and indoor temperature measurements.

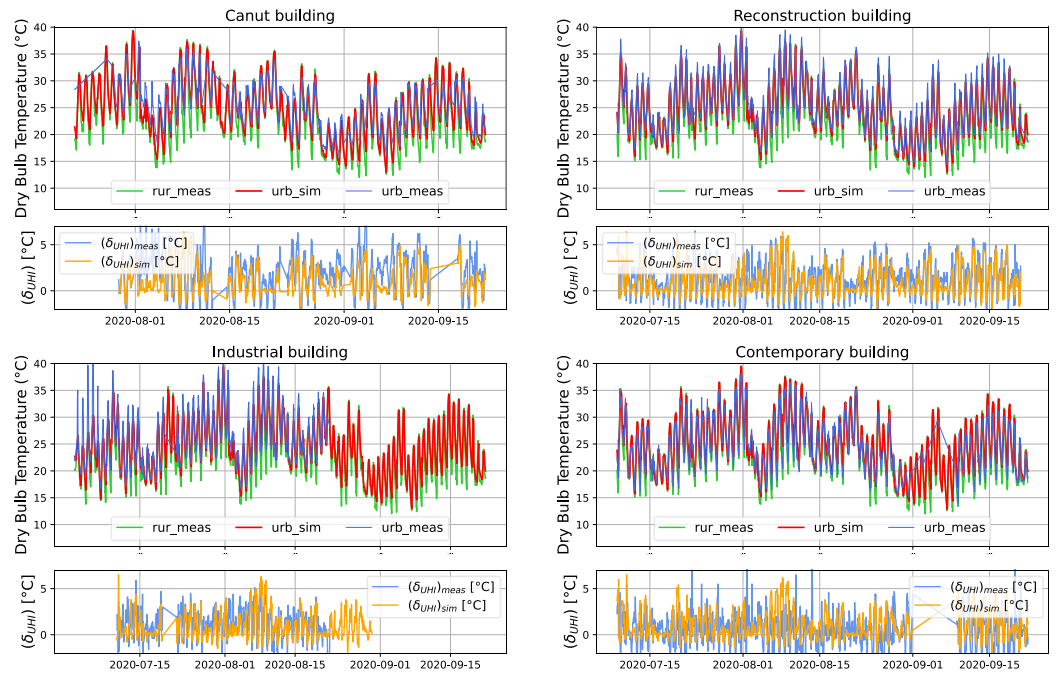
Table 2: Simulation parameters used to compute the UHI with UWG

Parameter	Canut	Industrial	Reconstruction	Contemporary
Building Height (m)	21	21	38	21
Building Density	0.43	0.33	0.29	0.19
Urban area vertical to horizontal ratio	1.27	0.98	1.21	0.55
Vegetation cover ratio	0.02	0.09	0.02	0.12
Tree Cover ratio	0.04	0.05	0.05	0.22

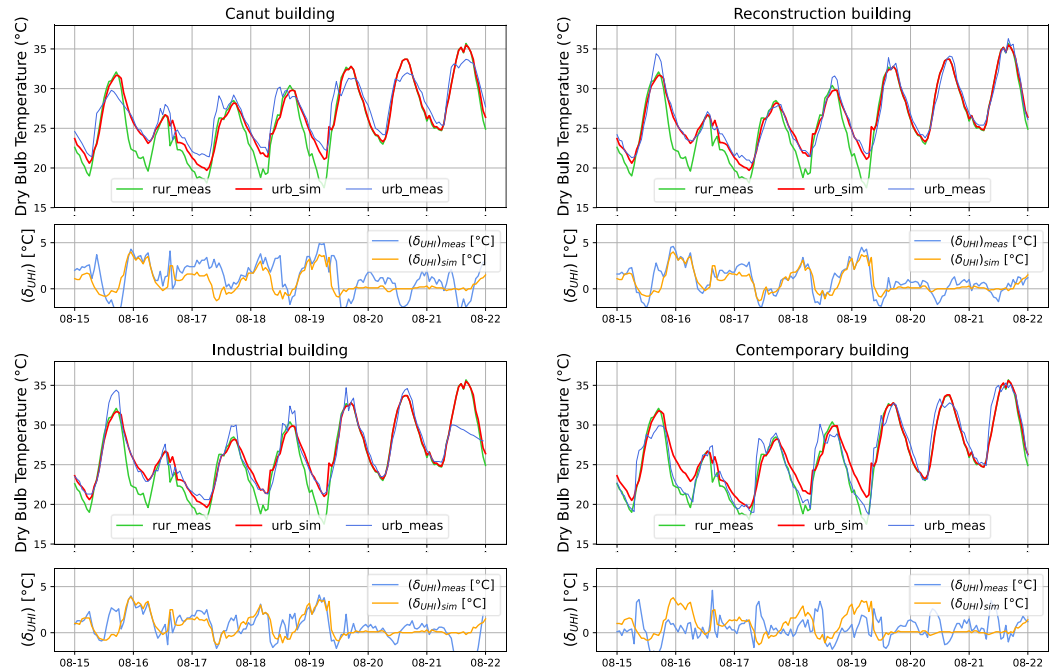
560 *6.2 Accuracy of the UWG Predictions*

Figures 7 and 8 show 2 graphs for each case study apartment. The upper graph shows outdoor air temperature values based on UWG predictions (red line), in situ measurements (blue line), and rural weather data (green line), while the bottom graph shows δ_{UHI} based on the measurements (blue line) and simulation predictions (orange line). Figure 7 shows the outdoor air temperature values from the beginning of the measurement period until the 22nd of September. Figure 8 focuses on the period between the 15th and 22nd of August.

The daytime/nighttime patterns of the UHI amplitude δ_{UHI} predicted with UWG were similar to those based on the measurements. During the daytime, δ_{UHI} predicted with UWG reached null. During the nighttime, when the measured δ_{UHI} value reached zero, the predicted δ_{UHI} value was also a null value (Figure 8, near the 20th of August, for example). The predicted nighttime UHI amplitudes were quite similar to those based on the measurements, despite a slight overestimation of the UHI predictions in the Contemporary-period case study (between the 5th and 10th of August, for example) and a slight underestimation in the Canut-period case study. These observations were confirmed by the average values of the predicted nighttime UHI amplitudes $(\overline{\delta_{UHI}})_{night}$ provided in Table 3.



580 *Figure 7: Outdoor air temperature in all test cases from July to September (top graph) (urban simulations (red), urban measurements (blue) and rural measurements (green)) and δ_{UHI} in the bottom graph (measured (blue lines) and simulated (orange lines) δ_{UHI} values)*



585 *Figure 8: Focus on the outdoor air temperature (top graph) in all case studies from the 15th to 22nd of August (urban simulations (red), urban measurements (blue) and rural measurements (green)) and δ_{UHI} in the bottom graph (measured (blue lines) and simulated (orange lines) δ_{UHI} values)*

The accuracy of the temperature predictions was quantified considering the distribution of the simulation error ε^T . The simulation error is the difference between the predicted and measured temperatures. In terms of the urban outdoor temperature:

590
$$\varepsilon_{o,urb}^T = (T_{o,urb})_{sim} - (T_{o,urb})_{meas}$$

The distributions of the errors exhibited bell-shaped curves. A curve not centered at 0 °C typically reveals a systematic error. A curve that is widely spread around its central value indicates a broad error range, which might be attributed to improper prediction of the temperature fluctuations. An ideal concordance between the predictions and measurements would correspond to a narrow distribution centered at 0 °C.

595

The distributions of the simulation errors during the nighttime $(\varepsilon_{o,urb}^T)_{night}$ in the four study cases are shown in Figure 9. Nighttime periods were arbitrarily set between 22:00 and 7:00. The average and RMSE of the nighttime error values are given in Table 3. In regard to the Canut-period building, the nighttime temperatures were underestimated, with an average error of -1.39 °C. Thus, the UHI amplitudes were underestimated near the Canut-period building, which is located in a dense district. In regard to the Contemporary-period building, the nighttime temperatures were slightly overestimated on average, with an average error of 0.73 °C, but the error distribution was quite broad, with an RMSE value of 0.98 °C. These discrepancies might be attributable to the presence of the Saone River close to the building, which cannot be modeled with the UWG model. The average and standard deviation of the errors were lower in the Industrial- and Reconstruction-period test cases.

There occurred errors between the outdoor predicted and measured temperatures. However, since the purpose of the UWG model was to correct weather data considering the effects of the urban fabric, the following question arises: does the UWG model truly refine the description of the outdoor thermal environment or does the model yield a worse result than that based on the considered rural data because of improper models or model settings? To answer this question, distributions of the nighttime UHI amplitudes $(\delta_{UHI})_{night}$ were visualized in the same graph as distributions of the simulation errors $(\varepsilon_{o,urb}^T)_{night}$. Average values of both $(\overline{\varepsilon_{o,urb}^T})_{night}$ and $(\overline{\delta_{UHI}})_{night}$ are listed in Table 3. Clearly, there occurred many more discrepancies between the measured rural and urban temperatures (a UHI amplitude of 2.31 °C on average) than those between the predicted and measured urban temperatures (an error of -0.36 °C on average). In conclusion, when appropriately parametrized, UWG improves the representation of the urban building outdoor environment.

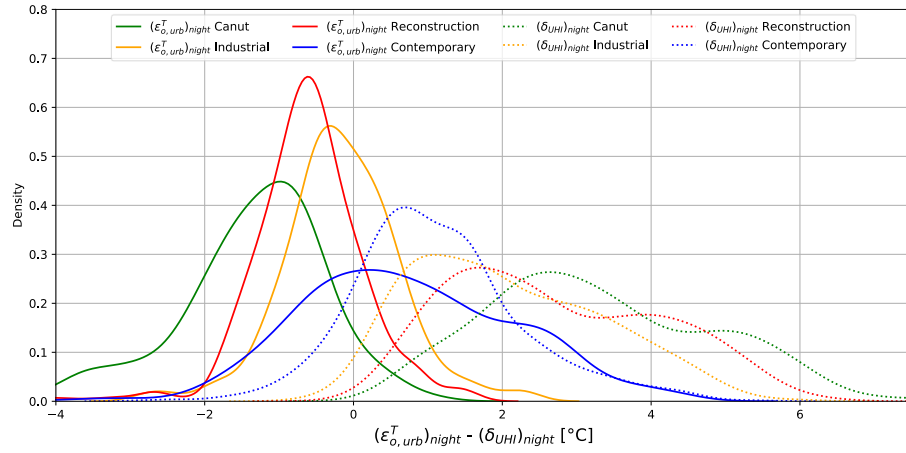


Figure 9: Distribution of the outdoor temperature error between the UWG predictions and measurements during the night $(\varepsilon_{o,urb}^T)_{night}$ (solid lines) and distribution of the measured UHI during the night $(\delta_{UHI})_{night}$ (dotted lines)

625

Table 3: Summary of the statistics on the outdoor temperature measurements and predictions

	Nighttime average data							
	UHI measured	UHI prediction	Simulation error - average	RMSE	Daily amplitude prediction	Daily amplitude measured	Simulation error - average	RMSE
	$(\overline{\delta_{UHI}})_{night}^{meas}$	$(\overline{\delta_{UHI}})_{night}^{sim}$	$(\overline{\varepsilon_{o,urb}^T})_{night}$		$\overline{\Delta T_{o,sim}}$	$\overline{\Delta T_{o,meas}}$	$(\overline{\varepsilon_{o,urb}^T})$	
Unit	[°C]	[°C]	[°C]	[°C]	[°C]	[°C]	[°C]	[°C]
Canut	3.34	1.95	-1.39	1.09	9.37	7	-1.12	1.97
Industrial	2.07	1.88	-0.16	0.44	9.69	12.2	-0.32	1.36
Reconstruction	2.72	2.11	-0.61	0.59	9.64	10.5	-0.36	1.14
Contemporary	1.12	1.85	0.73	0.98	9.85	10.2	0.37	1.79
Average value	2.31	1.95	-0.36	0.78	9.64	9.97	-0.36	1.56

6.3 Indoor Temperature Predictions

630 The evolution of the living room air temperature in the four case studies is shown in
Figures 10 and 11. The data in Figure 10 range from the beginning of the measurement
period until the 22nd of September. Figure 11 focuses on the period between the 12th
and 19th of September. The measurements are indicated in blue, and the simulation
635 predictions are indicated in red. The outdoor air temperature predicted with the UWG
model is indicated in light blue.

Figure 10 shows that the trends of the indoor temperature evolution were suitably
reproduced in the simulation predictions. The day-to-day mean temperature evolution
patterns were similar between the predictions and measurements. The curves did not
reveal any bias in the simulated temperatures. This observation is particularly important
640 because this suggests that the energy budget of the apartments involving all types of
thermal solicitations (solar radiation, outdoor air temperature, outdoor thermal
radiation, and indoor loads) was suitably reproduced on a daily average basis with the
simulation tool.

The day-to-day evolution patterns of the daily temperature fluctuations were suitably
645 reproduced most of the time, despite isolated events during which the measured
temperatures were lower at night than were the predicted temperatures. These
observations are confirmed by the data plotted in Figure 11. In regard to the Canut- and
Industrial-period apartments, the daily temperature fluctuations were slightly
underestimated. Regarding the Reconstruction- and Contemporary-period apartments,
650 the fluctuations were slightly overestimated.

The simulation error is the difference between the simulated and the measured
temperature:

$$\varepsilon_i^T = (T_i)_{sim} - (T_i)_{meas}$$

655 Table 4 provides statistics on the simulation error distributions computed with the
indoor daily mean temperature ε_i^{DMT} to assess the capability of the thermal tool chain
to accurately predict the day-to-day evolution of the average indoor temperature. The
daily average indoor temperature prediction error values ε_i^{DMT} mostly varied between

–0.5 °C and 0.5 °C. The mean of the root mean square error $rms_{\varepsilon_i^{DMT}}$ for all rooms was smaller than 1 °C.

660 The accuracy of the predictions was also quantified through the indoor temperature prediction error values ε_i^T . The distribution of the errors for each room of the four apartments is shown in Figure 12 (red curves). The average $\overline{\varepsilon_i^T}$ and root mean square $rms_{\varepsilon_i^T}$ values of these error distributions are given in Table 4. These statistics were computed based on error values ε_i over all the simulation experiments.

665 In regard to the Canut-, Industrial- and Reconstruction-period apartments, the error distributions were bell-shaped patterns with a unique peak located near zero (Figure 12, red curves). As expected, due to the heat released by washing machines, which was not modeled in the simulations, the maximum average and rms error values were found for the WC of the Canut-period apartment, with $\overline{\varepsilon_i^T} = -2.48$ °C and $rms_{\varepsilon_i^T} = 3.4$ °C.

670 Regarding the remaining apartment rooms, the average errors $\overline{\varepsilon_i^T}$ mostly varied between –0.5 °C and 0.5 °C, revealing a quasi-absence of bias. The root mean square errors $rms_{\varepsilon_i^T}$ mostly were smaller than 1.15 °C, with an even better precision in the Industrial-period building case.

In terms of the Contemporary-period building, the error distributions revealed a
675 secondary peak, and the average and rms error values were thus slightly higher for all the rooms except the living room. It was found that the simulations did not reproduce the distinctive temperature evolution patterns between the living zone (living rooms and kitchen) and night zone (bedrooms and bathrooms). The living zone was mono-oriented toward the south. The night zone was cross ventilated. During the day in the
680 night zone, the shutters were closed, leading to a smaller temperature increase. During the night, the windows were opened, leading to a temperature decrease. These two zones are separated by a single partition door. The intensity of the heat exchange process between these two zones depends on the opening percentage of the partition door. If the door is fully opened, advection through the door opening could homogenize
685 the temperature within the apartment. If the door is only slightly opened, two distinctive thermal behaviors could be expected in these two zones. The actual opening percentage of the partition door could not be captured by the contact sensor.

690 It should be mentioned that, given the level of fluctuations in the measured outdoor temperatures at the weather station located approximately 10 km away from the test case apartments and the potential number and variety of thermal phenomena affecting the temperature evolution between the weather station and apartment rooms, the level of precision reached by the simulations is remarkable.

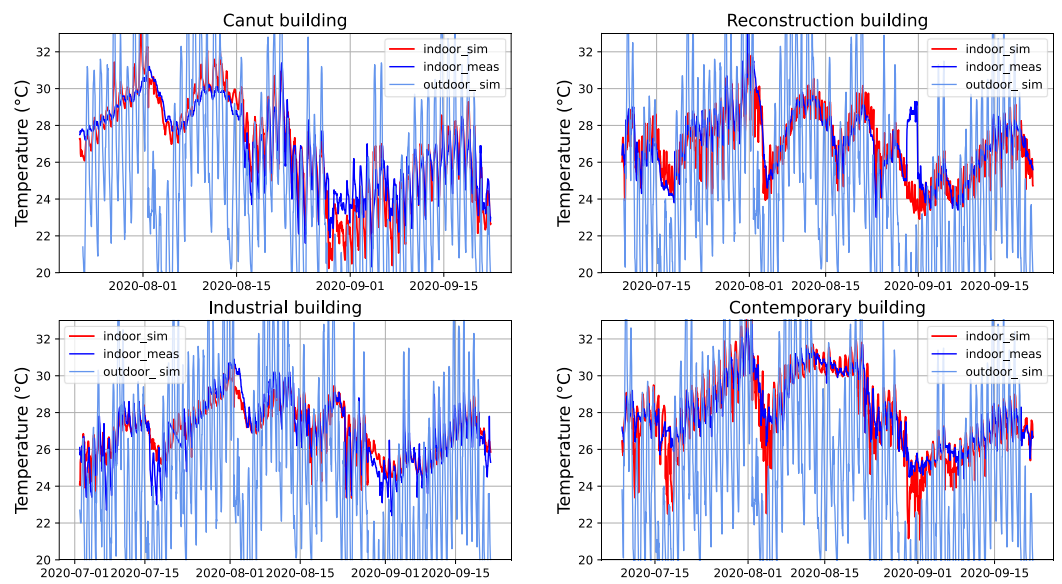


Figure 10: Simulated (red) and measured (blue) air temperatures in the living room and outside air temperature (light blue) from July to September

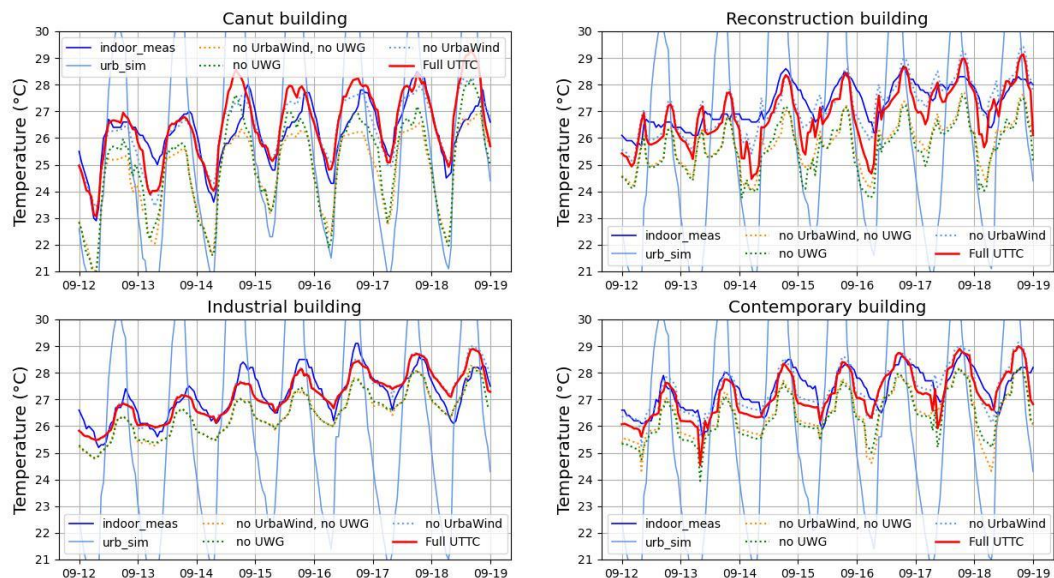


Figure 11: Focus on the simulated [full UTTC (red solid line), without UrbaWind (blue dotted line), without UWG (green dotted line), and only with EnergyPlus considering standard pressure coefficient and rural weather file values (yellow dotted line)] and measured (blue) living room air temperatures and the outside temperature (light blue) from the 12th to 19th of September

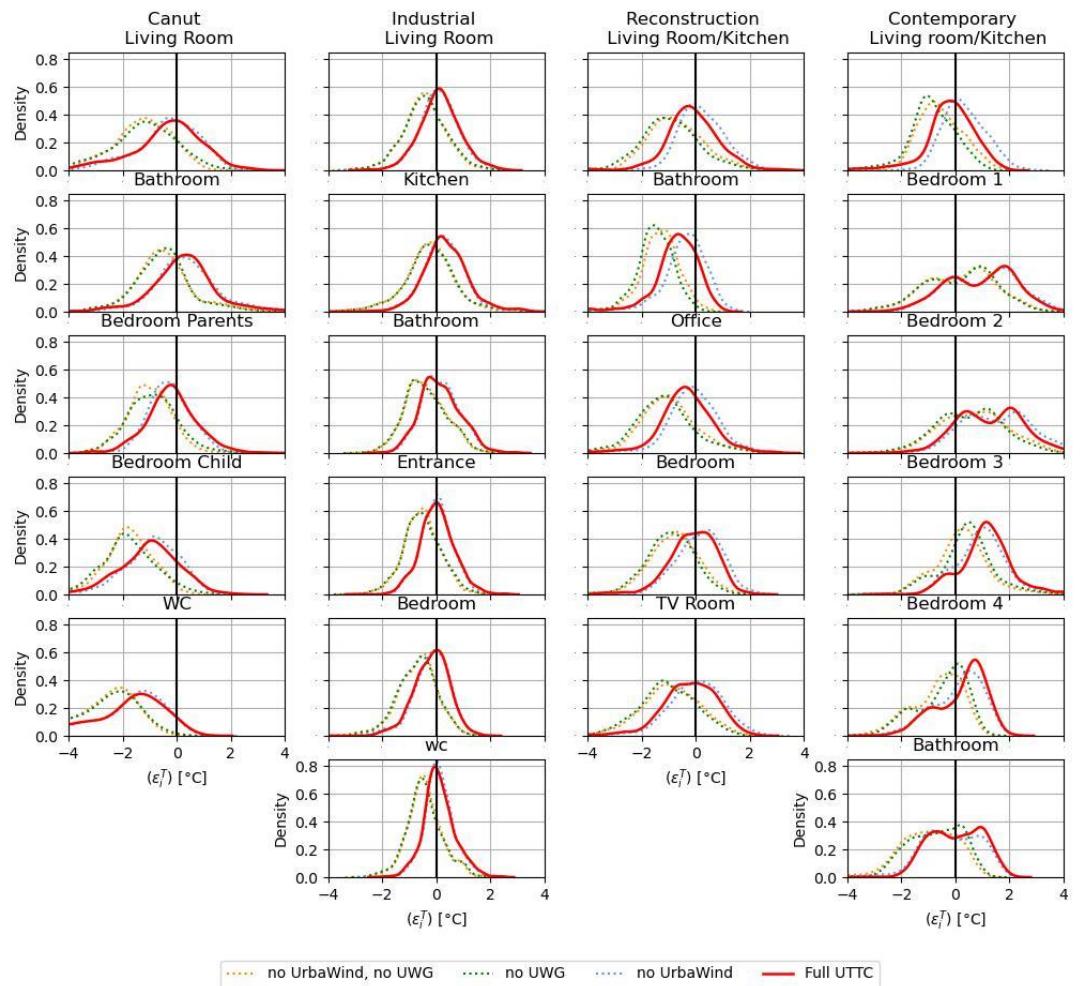


Figure 12: Distribution of the temperature error between the simulation predictions and measured temperature (ϵ_T^r) values for each room in each case study [full UTTC (red solid line), without UrbaWind (blue dotted line), without UWG (green dotted line), and only with EnergyPlus based on standard pressure coefficient and rural weather file values (yellow dotted line)]

Table 4: Statistics of the indoor temperature prediction errors

Period	Room	Hourly temperature		Daily mean temperature	
		$\overline{\varepsilon_i^T}$	$rms_{\varepsilon_i^T}$	ε_i^{DMT}	$rms_{\varepsilon_i^{DMT}}$
Canut	Living Room	-0.31	1.34	-0.01	0.8
	Bathroom	0.36	1.28	0.51	1.07
	Bedroom (Parents)	0.09	0.9	0.05	0.51
	Bedroom (Child)	-1.05	1.6	-0.78	1.13
	WC	-2.48	3.4	-1.97	2.44
	All Rooms Average	-0.69	1.7	-0.44	1.19
Industrial	Living Room	0.12	0.76	0.08	0.56
	Kitchen	0.35	0.93	0.24	0.61
	Bathroom	0.14	0.76	0.06	0.62
	Entrance	0.02	0.65	-0.03	0.52
	Bedroom	-0.19	0.68	-0.2	0.48
	WC	0.1	0.59	0.03	0.48
	All Rooms Average	0.09	0.73	0.03	0.55
Reconstruction	Living	-0.21	1.12	-0.27	0.91
	Room/Kitchen				
	Bathroom	-0.69	1.06	-0.59	0.87
	Office	-0.37	1.06	-0.41	0.78
	Bedroom	-0.12	0.87	-0.06	0.59
	TV Room	-0.25	1.06	-0.22	0.79
	All Rooms Average	-0.33	1.034	-0.31	0.79
Contemporary	Living	-0.18	0.94	-0.17	0.61
	Room/Kitchen				
	Bedroom 1	0.94	1.61	1.09	1.52
	Bedroom 2	1.29	1.78	1.4	1.73
	Bedroom 3	1.15	1.54	1.16	1.42
	Bedroom 4	0.2	0.96	0.27	0.77
	Bathroom	0.04	0.96	0.14	0.84
	All Rooms Average	0.57	1.30	0.65	1.15
Mean UTTC	Global Average	-0.05	1.17	0.015	0.91

6.4 Air Humidity

Figure 13 shows the evolution of the air specific humidity during the period between the 12th and 19th of September. The difference between the specific humidity measured at the rural weather station (green line) and the specific humidity measured in the living rooms (blue curves) was close to $0.002 \text{ kg}_w/\text{kg}_{da}$, which is very small. The water vapor sources and sinks in the urban environment and apartments did not greatly affect

the specific humidity. In the Canut- and Reconstruction-period apartments, the specific humidity was slightly lower than that in the rural area on average. In the Industrial- and Contemporary-period apartments, the specific humidity was slightly higher on average.

Compared to the rural values, UWG did not modify the air specific humidity (the light blue and green curves are similar). EnergyPlus did not modify the specific humidity values (red curves). Thus, by only performing small adjustments in the air specific humidity, the tool chain reproduced the quasi-absence of urban and building effects on this quantity well. The variations in relative humidity could therefore be more related to local temperature variations than to specific humidity variations.

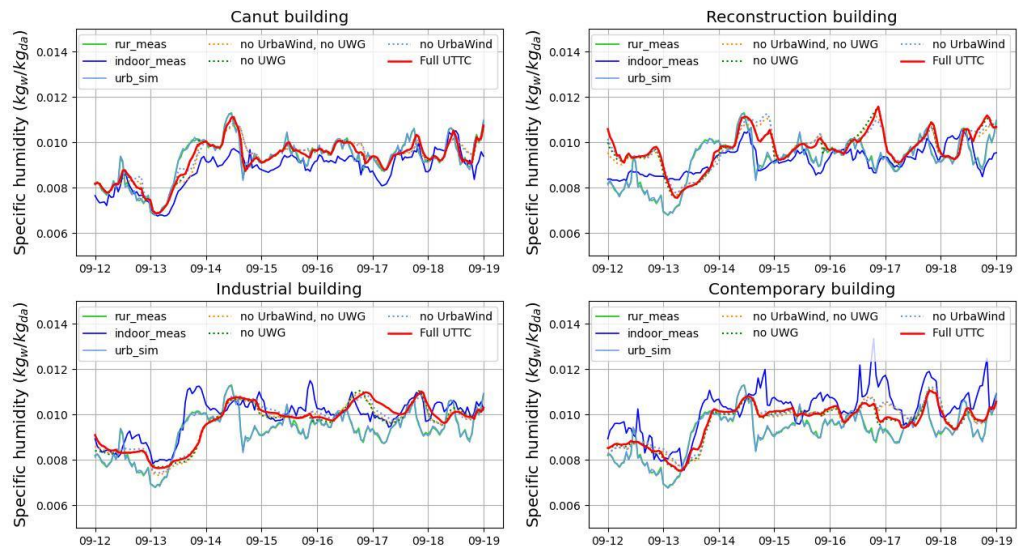


Figure 13: Focus on the simulated [full UTTC (red solid line), without UrbaWind (blue dotted line), without UWG (green dotted line), and only with EnergyPlus based on standard pressure coefficient and rural weather file values (yellow dotted line)] and measured (blue) living room air specific humidities and on the outdoor urban (light blue line) and rural (green line) air specific humidities measured from the 12th to 19th of September

7. Discussion

7.1 Pertinence of the UTTC

735 In the Urban Thermal Tool Chain, UWG and UrbaWind are employed to refine the outdoor thermal loads on the building of interest. In the previous section, the capacity of the UWG model to provide accurate outdoor temperature corrections was demonstrated. However, the impact of both outdoor simulation tools on the indoor predictions was not evaluated. As such, additional simulations were performed with
740 partial applications of the UTTC to individually evaluate the gain in precision due to each tool.

Figures 11, 12 and 13 show the simulation results obtained with the following partial applications of the UTTC: no UWG, no UrbaWind, and no UWG nor UrbaWind. When UWG was not applied (green and yellow dotted lines), the building simulation was fed
745 directly with the rural weather data. When UrbaWind was not employed (blue and yellow dotted lines), the default pressure coefficients proposed by DesignBuilder for sheltered wind exposition conditions were applied.

Figures 11 and 12 reveal that UrbaWind did not significantly impact the indoor temperature predictions. UrbaWind computes the pressure coefficient in front of
750 openings. This observation is unsurprising in mono-oriented apartments (Canut- and Industrial-period apartments), in which the gradient of the pressure loads among the windows is low, and the flow rate is mainly attributed to thermal ventilation. In the cross-ventilated apartments (Reconstruction- and Contemporary-period apartments), the airflow rate greatly depended on the pressure coefficient distribution among the
755 opened windows, and UrbaWind was expected to improve the prediction of these airflows. However, since the airflow rates reached in the cross-ventilated apartments were very high, the airflow-induced cooling effect could reach saturation. The higher the airflow rate, the closer the indoor air temperature is to the outdoor air temperature. Once the airflow rate reached a sufficient level, the indoor temperature already reached
760 a value approaching the outdoor temperature. Beyond this value, the indoor temperature no longer depended on the airflow rate, and UrbaWind could not further improve the

indoor temperature predictions. This conclusion might be true for the two cross-ventilated test case apartments in the present study. The saturation effect must be further investigated. The two cross-ventilated test case apartments in the present study are, compared to the other urban apartments, suitably exposed to wind flow: the Contemporary-period apartment is located on the last floor of the building, and the Reconstruction-period apartment is located in a building that is significantly higher than the surrounding buildings. To assess the value of UrbaWind in the proposed UTTC, further investigations should be conducted on more sheltered apartments, such as those on lower floors within dense districts.

Figures 11 and 12 reveal that UWG application exerted a clear impact on the indoor temperature predictions. There occurred a constant bias of approximately 1 °C between the simulation results obtained with and without the UWG model. This bias was clearly observed in the error distribution curves (Figure 12), which were all shifted toward the left by approximately 1 °C. By increasing the outdoor temperature during the night, the UWG model simulates the reduction in the cooling potential of the buildings. Not employing UWG could result in overpredicting this cooling potential.

As expected, the application of UrbaWind and UWG exerted no impact on the specific humidity predictions (Figure 13).

7.2 Key Simulation Parameters

The number of parameters needed to establish a thermal model of a given urban building with the UTTC is consequential. Obviously, certain parameters may exert little impact on the indoor temperature predictions, whereas other parameters may exert a notable impact on these predictions. The latter parameters are referred to as key simulation parameters. The rigorous technique to identify key simulation parameters is sensitivity analysis. This technique was not applied in this study. However, during the analysis of the measurements and calibration of the simulations, certain key simulation parameters were clearly identified. This section inventories these identified key parameters.

790 One key parameter is the night time urban boundary layer height $h_{ubl,night}$ provided to UWG. Since there are no clear guidelines available to set the value of $h_{ubl,night}$, several values were tested between 20 m and 500 m. The best outdoor simulation results were obtained for $h_{ubl,night} = 30$ m.

Figure 14 shows the outdoor temperature error $(\epsilon_{o,urb}^T)_{night}$ distributions based on 795 the UWG simulation results obtained for $h_{ubl,night} = 30$ m and $h_{ubl,night} = 150$ m. Setting the urban boundary layer height away from its optimal value resulted in a very wide spread of the temperature errors.

The urban boundary layer height is the height of the urban boundary layer. The urban boundary layer is defined by climate scientists as the volume of air within which vertical 800 heat exchange and momentum exchange coming from the urban surface occur. Hot air is blocked by a temperature inversion at the urban boundary layer height. With this rigorous definition of the urban boundary layer height, the optimal value $h_{ubl,night} = 30$ m is too small to be physically realistic. The discrepancy between the physically realistic values of $h_{ubl,night}$ and the optimal value of $h_{ubl,night}$ given to UWG might 805 come from the extreme simplicity of the urban boundary layer model in UWG.

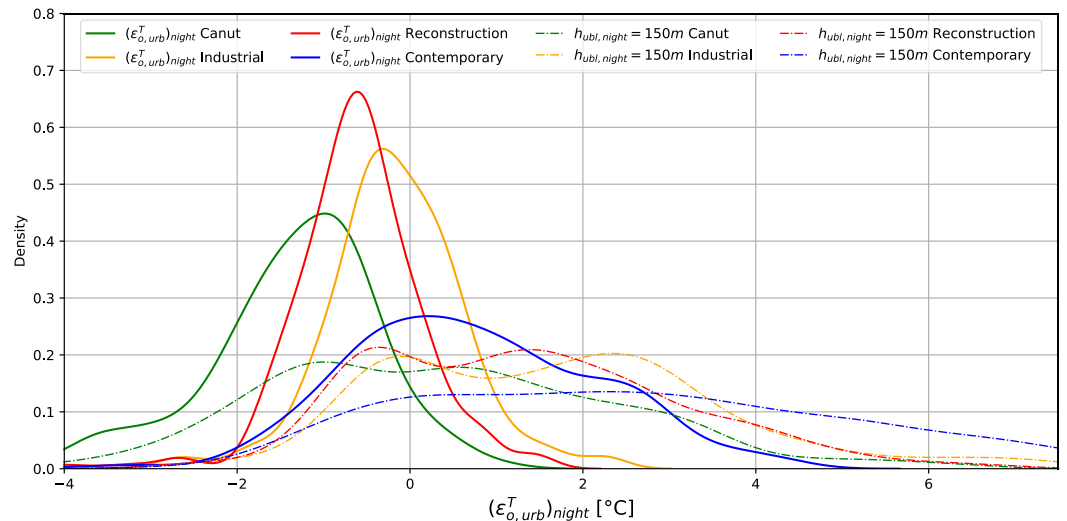


Figure 14: Distribution of the outdoor temperature error between the UWG predictions and measurements during the night $(\varepsilon_{o,urb}^T)_{night}$ [the solid lines indicate the final parametrization of UWG ($h_{ubl,night} = 30$ m), and the dash-dotted lines indicate an urban boundary layer height of $h_{ubl,night} = 150$ m]

810 Analysis of the indoor measurement results according to the data displayed in Figure 5 identified the window opening schedule as a key simulation parameter. The different opening schedules observed during the measurement campaign resulted in varying indoor temperature regimes. The quality of the reproduction window opening schedules may be evaluated at two levels: the daily duration of the opening state and the
815 instantaneous opening state. If the parametrized daily durations of the window opening state are excessively long or short, the apartment daily heat balance is unbalanced, which results in a bias in the day-to-day mean temperature. Additionally, the indoor air temperature is quickly adjusted versus the outdoor air temperature after window opening. If an error is made regarding the instantaneous opening state, this could result
820 in an error in the temperature predictions, which could be elevated in amplitude but short in duration.

The blind operating schedule was also a key simulation parameter. Figure 15 shows the impact of considering different blind schedules on the indoor temperature predictions for the living room of each apartment. The solid lines indicate the
825 distribution of the indoor temperature errors obtained with the blind schedules constructed based on the interviews of the occupants. The dashed lines indicate the distribution of the error considering a standard blind schedule. In this schedule, the blinds remain closed on all the weekdays during the night from 10 pm to 7 am and during the day from 9 am to 5 pm. On all of the weekend days, the blinds remain closed
830 only during the night from 11 pm to 9 am. Except for the Industrial-period case study, the error with the standard blind schedules was greater than that with the schedules created based on the interviews. The distributions were more widely spread and less centered at 0 °C, except for the Industrial-period apartment for which the distribution was more concentrated. Both types of blind schedules for this apartment were similar,
835 explaining this small difference in the error distribution.

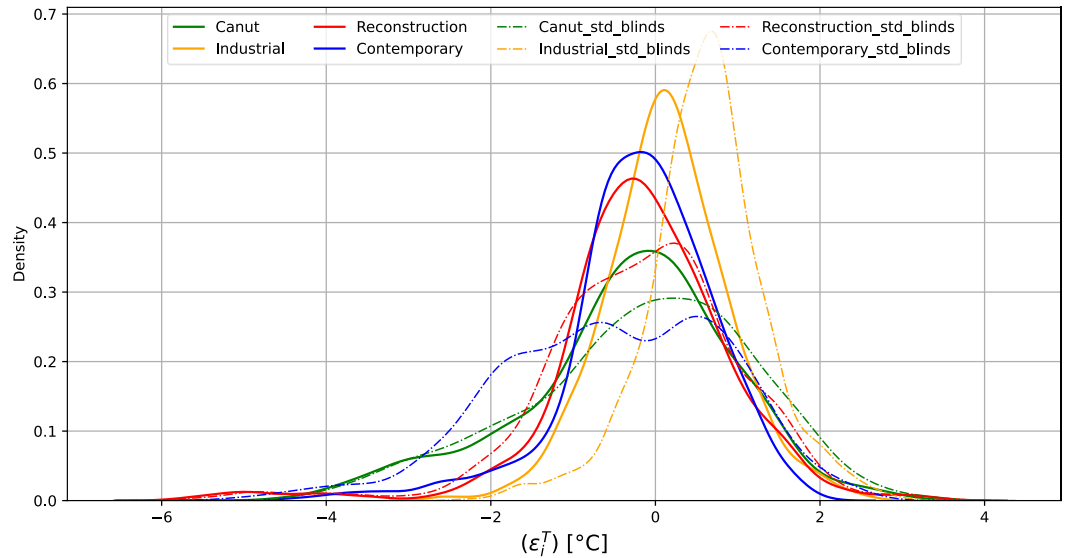


Figure 15: Distribution of the living room temperature error between the simulation predictions and measured temperature values (ϵ_l^T) for each apartment under the different blind schedules [the solid lines indicate the final parametrization of UWG (the blind schedule built based on the interviews), and the dash-dotted lines indicate the results with standard blind schedules]

840

7.3 Required Measurements for Model Calibration

In the previous section, three key simulation parameters were identified. These parameters are dynamic and evolve over time. If proper model calibration would be accomplished with the UTTC, the values of these three key simulation parameters should be recorded.

845

One of the initial intentions of the measurement campaign was to continuously measure every opening state with contact sensors. Beyond the fact that the sensors attached to the blinds did not function at all, there existed a notable limitation of the contact sensor: these sensors only detected two opening states. However, occupants might wish to partially open their windows to better control the airflow rate or partially

850

open blinds to finely customize the trade-off between natural light and sun warmth. To capture the above fine tuning phenomenon, progressive opening sensors may have to be developed. These sensors should be suitable for in situ measurements.

855 The appropriate sensor to continuously measure the urban boundary layer height is the ceilometer. Indeed, certain ceilometers can compute boundary layer heights based on vertical particle concentration profiles. Ceilometers are expensive and bulky, and these instruments require an unobstructed view of the sky. These devices are difficult to conceive as part of an in situ measurement setup, but ceilometer measurements could be generalized at the city scale.

860 **8. Conclusion**

This paper presented a new simulation tool chain belonging to a new category of simulation tools denoted as urban thermal tool chains, or UTTC. The simulation tool was developed to accurately and quickly simulate the indoor comfort conditions in passive urban buildings under hot summer conditions. As such, this tool accurately 865 modeled all the prevailing heat transfer rates around and within the buildings of interest. This tool further simulated the effects of the urban environment on the prevailing heat transfer rates.

To assess the accuracy of the UTTC, an extensive in situ measurement campaign was conducted during the summer of 2020 in the city of Lyon, and the UTTC 870 predictions were compared to the measurement data. The comparison revealed a remarkable capacity of the UTTC to accurately predict the indoor air temperature and humidity. Even if rigorous scientific reasoning would limit the validity of the model within the perimeter of the four test cases investigated, there exists a high probability that many urban building configurations could be simulated accurately with the UTTC.

875 The study of the pertinence of the UTTC demonstrated that not applying the UWG could result in overpredicting the cooling potential of passive buildings during summer. There indeed occurred a constant bias of approximately 1 °C between the simulation results obtained with and without the UWG model. Regarding the two cross-ventilated apartments in this study, the results revealed that UrbaWind did not significantly impact

880 the indoor temperature predictions. However, further testing of more sheltered
apartments could be required to better highlight the pertinence of UrbaWind pressure
coefficient evaluation.

The assessment of the comfort predictions was purely based on the air temperature
and humidity predictions. Even if other parameters, such as the air velocity or wall
885 temperature, may influence the comfort level, the air temperature remains the prevailing
parameter to evaluate comfort ([35] Parsons, 2002; page 2). We assumed that if the air
temperature is satisfactorily predicted, the possibility that the surface temperatures were
also suitably predicted is high. The air velocity within rooms is more difficult to predict,
especially if occupants employ individual fans.

890 The UTTC is now an operational and user-friendly tool capable of addressing future
indoor thermal issues attributed to heat waves in cities. This widens the scope for future
exciting research on this subject.

Declaration of Competing Interests

The authors declare that they have no known competing financial interests or
895 personal relationships that could have appeared to influence the work reported in this
paper.

Acknowledgments

The authors gratefully acknowledge the Ecole Urbaine de Lyon (EUL) for funding
the sensors employed in this study and the IMU – CoCoVN lab for funding the initial
900 UTTC research described in this paper.

The authors wish to thank the residents of the four case study apartments who
allowed measurement of all the quantities required in this study during the summer of
2020.

References

- 905 [1] <https://data.worldbank.org/indicator/SP.URB.TOTL.IN.ZS>
- [2] Santamouris, M., 2018. Cooling Energy Solutions For Buildings And Cities. World Scientific Publishing Co Pte Ltd, New Jersey.
- [3] Fabi, V., Andersen, R.V., Corgnati, S., Olesen, B.W., 2012. Occupants' window opening behaviour: A literature review of factors influencing occupant behaviour and models. Building and Environment 58, 188–198. <https://doi.org/10.1016/j.buildenv.2012.07.009>
- 910 [4] Bui, R., Labat, M., Lorente, S., 2019. Impact of the occupancy scenario on the hygrothermal performance of a room. Building and Environment 160, 106178. <https://doi.org/10.1016/j.buildenv.2019.106178>
- [5] Hong, T., Yan, D., D'Oca, S., Chen, C., 2017. Ten questions concerning occupant behavior in buildings: The big picture. Building and Environment 114, 518–530.
- 915 <https://doi.org/10.1016/j.buildenv.2016.12.006>
- [6] Mavrogianni, A., Davies, M., Taylor, J., Chalabi, Z., Biddulph, P., Oikonomou, E., Das, P., Jones, B., 2014. The impact of occupancy patterns, occupant-controlled ventilation and shading on indoor overheating risk in domestic environments. Building and Environment 78, 183–198. <https://doi.org/10.1016/j.buildenv.2014.04.008>
- 920 [7] Piselli, C., Pisello, A.L., 2019. Occupant behavior long-term continuous monitoring integrated to prediction models: Impact on office building energy performance. Energy 176, 667–681. <https://doi.org/10.1016/j.energy.2019.04.005>
- [8] Levermore, G.J., A.M. Jones, and A.J. Wright, Simulation of a Naturally Ventilated Building at Different Locations. ASHRAE Transactions, 2000. Vol. 106 (Part 2)
- 925 [9] Solar Energy Laboratory, TRANSSOLAR, CSTB, et TESS. « TRNSYS 16 Documentation - Multizone Building Modeling with Type56 and TRNBuild », 2007.
- [10] U.S. Department of energy. « EnergyPlus Version 8.9.0 Documentation - Engineering Reference », 2014.
- [11] Bueno, B., Norford, L., Hidalgo, J., Pigeon, G., 2013. The urban weather generator. Journal of Building Performance Simulation 6, 269–281. <https://doi.org/10.1080/19401493.2012.718797>
- 930 [12] Grimmond, C. S. B., M. Blackett, M. J. Best, J. Barlow, J-J. Baik, S. E. Belcher, S. I. Bohnenstengel, et al. « The International Urban Energy Balance Models Comparison Project: First Results from Phase 1 ». *Journal of Applied Meteorology and Climatology* 49, n° 6 (16 février 2010): 1268-92. <https://doi.org/10.1175/2010JAMC2354.1>.
- 935 [13] Ferreira, M.J., de Oliveira, A.P., Soares, J., Codato, G., Bárbaro, E.W., Escobedo, J.F., 2012. Radiation balance at the surface in the city of São Paulo, Brazil: diurnal and seasonal variations. Theor Appl Climatol 107, 229–246. <https://doi.org/10.1007/s00704-011-0480-2>
- [14] Musy, Marjorie, Laurent Malys, Benjamin Morille, et Christian Inard. « The Use of SOLENE-Microclimat Model to Assess Adaptation Strategies at the District Scale ». Urban Climate, Cooling Heat Islands, 14 (1 décembre 2015): 213-23. <https://doi.org/10.1016/j.uclim.2015.07.004>
- 940 [15] Gros, Adrien, Emmanuel Bozonnet, Christian Inard, et Marjorie Musy. « Simulation Tools to Assess Microclimate and Building Energy – A Case Study on the Design of a New District ». Energy and

- Buildings, SI: Countermeasures to Urban Heat Island, 114 (15 février 2016): 112-22. <https://doi.org/10.1016/j.enbuild.2015.06.032>
- 945 [16] Bruse, Michael, et Heribert Fleer. « Simulating Surface–Plant–Air Interactions inside Urban Environments with a Three Dimensional Numerical Model ». *Environmental Modelling & Software* 13, n° 3 (1 octobre 1998): 373-84. [https://doi.org/10.1016/S1364-8152\(98\)00042-5](https://doi.org/10.1016/S1364-8152(98)00042-5).
- [17] Robinson, Darren, Frédéric Haldi, Philippe Leroux, Diane Perez, Adil Rasheed, et Urs Wilke. « CITYSIM: Comprehensive Micro-Simulation of Resource Flows for Sustainable Urban Planning ». Proceedings of the Eleventh International IBPSA Conference, 2009. <http://infoscience.epfl.ch/record/148717>.
- 950 [18] Frayssinet, Loïc. « Adapter les modèles de chauffage et climatisation des bâtiments en puissance à l'échelle du quartier », 2018.
- [19] Masson, V., 2000. A Physically-Based Scheme For The Urban Energy Budget In Atmospheric Models. *Boundary-Layer Meteorology* 94, 357–397. <https://doi.org/10.1023/A:1002463829265>
- 955 [20] Bueno, B., Pigeon, G., Norford, L.K., Zibouche, K., Marchadier, C., 2012. Development and evaluation of a building energy model integrated in the TEB scheme. *Geosci. Model Dev.* 5, 433–448. <https://doi.org/10.5194/gmd-5-433-2012>
- [21] Ali-Toudert, F., Böttcher, S., 2018. Urban microclimate prediction prior to dynamic building energy modelling using the TEB model as embedded component in TRNSYS. *Theor Appl Climatol* 134, 1413–1428. <https://doi.org/10.1007/s00704-018-2621-3>
- 960 [22] Van Hooff, T., et B. Blocken. « On the effect of wind direction and urban surroundings on natural ventilation of a large semi-enclosed stadium ». *Computers & Fluids* 39, no 7 (1 août 2010): 1146-55. <https://doi.org/10.1016/j.compfluid.2010.02.004>.
- 965 [23] Fahssis, Karim, Guillaume Dupont, et P. Leyronnas. « UrbaWind, a Computational Fluid Dynamics Tool to Predict Wind Resource in Urban Area », 2010. [/paper/UrbaWind%2C-a-Computational-Fluid-Dynamics-tool-to-in-FAHSSIS-Dupont/7ebcb7488b8074e6c32dfac951eac44bd85d7fda](https://paperkit.net/paper/UrbaWind%2C-a-Computational-Fluid-Dynamics-tool-to-in-FAHSSIS-Dupont/7ebcb7488b8074e6c32dfac951eac44bd85d7fda).
- [24] Lauzet, Nicolas, Auline Rodler, Marjorie Musy, Marie-Hélène Azam, Sihem Guernouti, Dasaraden Mauree, et Thibaut Colinart. 2019. « How Building Energy Models Take the Local Climate into Account in an Urban Context – A Review ». *Renewable and Sustainable Energy Reviews* 116 (décembre): 109390. <https://doi.org/10.1016/j.rser.2019.109390>.
- 970 [25] Merlier, L., Frayssinet, L., Kuznik, F., Rusaouen, G., Johannes, K., Hubert, J.-L., Milliez, M., Lyon, Univ, de Lyon, I., Lyon, Université, 2017. Analysis of the (urban) microclimate effects on the building energy behaviour 8.
- 975 [26] Yang, X., Zhao, L., Bruse, M., Meng, Q., 2012. An integrated simulation method for building energy performance assessment in urban environments. *Energy and Buildings* 54, 243–251. <https://doi.org/10.1016/j.enbuild.2012.07.042>
- [27] Salvati, A., Roura, H.C., Cecere, C., 2015. URBAN MORPHOLOGY AND ENERGY PERFORMANCE: THE DIRECT AND INDIRECT CONTRIBUTION IN MEDITERRANEAN CLIMATE 8.
- 980 [28] Palme, M., Inostroza, L., Villacreses, G., Lobato-Cordero, A., Carrasco, C., 2017. From urban climate to energy consumption. Enhancing building performance simulation by including the urban heat island effect. *Energy and Buildings* 145, 107–120. <https://doi.org/10.1016/j.enbuild.2017.03.069>

- 985 [29] Bueno, B., Norford, L., Pigeon, G., Britter, R., 2011. Combining a Detailed Building Energy Model
with a Physically-Based Urban Canopy Model. *Boundary-Layer Meteorol* 140, 471–489.
<https://doi.org/10.1007/s10546-011-9620-6>
- [30] Google Maps. (2021). *Lyon*. Retrieved from
<https://www.google.fr/maps/@45.7725035,4.8493709,5592m/data=!3m1!1e3>
- 990 [31] Pascal, M., Laaidi, K., Ledrans, M., Baffert, E., Caserio-Schönemann, C., Le Tertre, A., Manach, J.,
Medina, S., Rudant, J., Empereur-Bissonnet, P., 2006. France’s heat health watch warning system. *Int J*
Biometeorol 50, 144–153. <https://doi.org/10.1007/s00484-005-0003-x>
- [32] Taesler, R., Andersson, C., 1984. A method for solar radiation computations using routine
meteorological observations. *Energy and Buildings* 7, 341–352. [https://doi.org/10.1016/0378-](https://doi.org/10.1016/0378-7788(84)90080-X)
[7788\(84\)90080-X](https://doi.org/10.1016/0378-7788(84)90080-X)
- 995 [33] Open Data of the Métropole of Lyon. <https://data.grandlyon.com/>
- [34] Rochard, Ulrich, Shanthirablan, Santhiah, Brejon, Camille, Chateau le Bras, Maëlle, 2015. Bâtiment
résidentiels: typologie du parc existant et solutions exemplaires pour la rénovation énergétique en France.
Rodler, A., Guernouti, S., Musy, M., Bouyer, J., 2018. Thermal behaviour of a building in its
environment: Modelling, experimentation, and comparison. *Energy and Buildings* 168, 19–34.
1000 <https://doi.org/10.1016/j.enbuild.2018.03.008>
- [35] Parsons, K., 2002. *Human Thermal Environments: the Effect of Hot, Moderate and. CRC Press, London.*